Possible improvements in SEMM-based joint identification

M. Di Manno [1], **J. Brunetti** [2], **W. D'Ambrogio** [2], **A. Fregolent** [1], **F. Latini** [1]
[1] Università di Roma La Sapienza, Dipartimento di Ingegneria Meccanica e Aerospaziale,
Via Eudossiana 18, 00184 Rome, Italy
e-mail: **matteo.dimanno@uniroma1.it**

[2] Università dell'Aquila, Dipartimento di Ingegneria Industriale e dell'Informazione e di Economia,
Via G. Gronchi 18, 67100 L'Aquila (AQ), Italy

Abstract
When dealing with complex mechanical systems, a challenging issue is the characterization of the mechanical properties of the joints that connect the subsystem components. This can be performed in the frame of Dynamic Substructuring by considering the joint as an independent subsystem. Its dynamic behavior can be identified starting from the known dynamics of the assembled system and from that of the connected subsystems using direct decoupling. If the connecting interface is not accessible to measurements, the expansion technique System Equivalent Model Mixing can be used to obtain the FRFs of the system at unmeasured DoFs from measurements at accessible DoFs. The identification process is affected by ill-conditioning thus the error in the data is largely amplified in the identified joint FRFs. In this work, the sources of ill-conditioning are investigated and some strategies to limit the error propagation in the solution are proposed. Experiments are carried out on a laboratory testbed to validate the effectiveness of the proposed strategies.

1 Introduction

Complex mechanical systems are composed of subsystems connected through different types of joints. It can be useful to identify the mechanical properties of the joints to highlight their effects on the dynamics of the whole system [1]. The identification of the dynamic behavior of the joints can be performed in the frame of experimental dynamic substructuring [2] using direct decoupling [3, 4]. The joint can be considered as an independent subsystem whose dynamic behavior can be identified starting from the known dynamics of the assembled system and from that of the subsystems connected by the joint. However, ill-conditioning issues may arise in the decoupling process, as it happens in most of inverse problems. Consequently, the identification can be prone to large amplification of the errors present in the data. The crucial choice of a proper set of DoFs to be used in the decoupling procedure is investigated in [5].

The joint identification procedure, through decoupling, requires information of the assembled system at least at the coupling DoFs, that are those physically connecting the joint to the other subsystems. Generally, the joint interface is not accessible for measurements, so expansion technique can be used to obtain the FRFs of the system at unmeasured DoFs from measurements at accessible DoFs. The System Equivalent Model Mixing (SEMM) [6] performs the expansion by combining the numerical and the experimental models of a component to obtain a hybrid model in which the experimental dynamics measured at accessible DoFs are expanded at inaccessible DoFs. In [7], the inaccessible dove-tail joint of a bladed disk structure is analyzed and the SEMM technique is implemented as an iterative procedure [8] to identify the properties of the connection. To reach a convergence in a small number of iteration, the SEMM procedure is performed introducing a higher weight on the coupling DoFs with respect to the other DoFs of the assembled system. However, the identified FRFs of the joint are largely affected by spurious peaks. In [9], the so called correlated SEMM is introduced to limit the error of the data, by removing the lowest correlated measurement channels from the set of experimental DoFs that are used to perform the SEMM expansion. Another technique to deal with ill-conditioned problems is the Truncated Singular Value Decomposition (TSVD) which

is used in [10] to improve the results of the expansion procedure within SEMM.

In this work, an analysis of the sources of ill-conditioning in the proposed identification procedure is made. The effect of different types of decoupling interfaces [11] on the estimation of the joint FRFs is analyzed. Moreover, the role of the weighted pseudo-inverse proposed in [7] on the conditioning of the procedure is investigated by analyzing the effect of the weights on the matrices to be inverted. Some strategies to limit the error propagation in the solution are proposed. In particular, an indication about the appropriate number of singular values to be truncated using TSVD is suggested. To estimate the properties of the identified joint, a fitting of the dynamic stiffness matrix of the joint is proposed. Experimental tests are carried out on a laboratory testbed derived from the one used in [12, 13] to assess the effectiveness of the proposed strategies.

2 Theoretical background

In this Section, the methods used to obtain the Frequency Response Functions (FRFs) of the joint are described. In particular, the theory of substructure decoupling and the SEMM method are recalled and fitted to the joint identification procedure, that is outlined in Section 2.3.

2.1 Substructure decoupling

Substructure decoupling allows to identify the dynamic behavior of an unknown substructure U (N_U DoFs) starting from the known assembled system RU and from the known information about a residual substructure R (N_R DoFs). The unknown substructure U and the residual substructure R are connected through a set of coupling DoFs. The DoFs of the assembled system RU can be partitioned into internal DoFs (u) (not belonging to the couplings) of substructure U, internal DoFs (r) of substructure R and coupling DoFs (c).

In direct decoupling, the unknown substructure U is identified by adding to the assembled system RU a fictitious substructure with an FRF opposite in sign to that of the residual subsystem R. The equations of motion can be written as:

$$\mathbf{u} = \mathbf{Y}(\mathbf{f} + \mathbf{g}) \tag{1}$$

with

$$\mathbf{Y} = \begin{bmatrix} \mathbf{Y}^{\mathrm{RU}} & \\ & -\mathbf{Y}^{\mathrm{R}} \end{bmatrix}, \quad \mathbf{u} = \begin{Bmatrix} \mathbf{u}^{\mathrm{RU}} \\ \mathbf{u}^{\mathrm{R}} \end{Bmatrix}, \quad \mathbf{f} = \begin{Bmatrix} \mathbf{f}^{\mathrm{RU}} \\ \mathbf{f}^{\mathrm{R}} \end{Bmatrix}, \quad \mathbf{g} = \begin{Bmatrix} \mathbf{g}^{\mathrm{RU}} \\ \mathbf{g}^{\mathrm{R}} \end{Bmatrix} \tag{2}$$

where $\mathbf{u}$ is the response vector, $\mathbf{f}$ is the external force vector, $\mathbf{g}$ is the vector of connecting forces between system and $\mathbf{Y}$ is the FRF.
In order to decouple the substructures, compatibility and equilibrium conditions must be satisfied at the interface between the assembled structure RU and the negative residual substructure R. Such interface includes both the coupling DoFs between substructures U and R and all the internal DoFs of substructure R. Note that it is necessary to use a number of interface DoFs greater or equal than the number of coupling DoFs c. As explained in [11], four possible types of interfaces can be used:

- standard interface, including only the coupling DoFs (c) between subsystems U and R;
- extended interface, including also a subset of internal DoFs ($i \subseteq r$) of subsystems R;
- mixed interface, including subsets of coupling DoFs ($d \subset c$) and internal DoFs ($i \subset r$);
- pseudo-interface, including only internal DoFs ($i \subseteq r$) of subsystems R.

The compatibility condition at the interface DoFs implies that any pair of matching DoFs u_l^{RU} and u_m^R i.e. DoF l on substructure RU and DoF m on substructure R have the same displacement, that is $u_l^{RU} - u_m^R = 0$. This condition can be generally expressed by introducing the signed boolean matrix $\mathbf{B}$:

$$\mathbf{B}\mathbf{u} = 0 \tag{3}$$

The equilibrium condition states that for any pair of interface DoFs, the interface forces must be equal and opposite in sign, i.e. $g_l^{RU} + g_m^R = 0$. Using the dual assembly, equilibrium is satisfied exactly by defining a

unique set of disconnection force intensities $\boldsymbol{\lambda}$:

$$\mathbf{B}^T\boldsymbol{\lambda} = -\mathbf{g} \tag{4}$$

By substituting the interface forces $\mathbf{g}$ from Eq. (4) into Eq. (1), the following system of equations is obtained:

$$\begin{cases} \mathbf{u} = \mathbf{Y}(\mathbf{f} - \mathbf{B}^T\boldsymbol{\lambda}) \\ \mathbf{B}\mathbf{u} = \mathbf{0} \end{cases} \tag{5}$$

It is possible to eliminate $\boldsymbol{\lambda}$ and obtain the single line equation:

$$\mathbf{u} = \bar{\mathbf{Y}}\mathbf{f} \tag{6}$$

in which $\bar{\mathbf{Y}}$ (or better, a submatrix of $\bar{\mathbf{Y}}$) is the frequency response function of the unknown subsystem:

$$\bar{\mathbf{Y}} = \mathbf{Y} - \mathbf{Y}\mathbf{B}^T(\mathbf{B}\mathbf{Y}\mathbf{B}^T)^{-1}\mathbf{B}\mathbf{Y} \tag{7}$$

The term $\mathbf{B}\mathbf{Y}\mathbf{B}^T$ in Eq. (7) is the Interface Flexibility Matrix (IFM) that depends on the selected interface. Since this matrix has to be inverted, care must be taken if it is ill-conditioned to limit the error propagation in the solution. Note that to find the FRF of subsystem U at a subset of coupling DoFs c and/or internal DoFs u, it is necessary to measure these DoFs in the whole system RU.

Direct decoupling can be used for joint identification. In this case, the joint J is considered as an independent subsystem with given mass and stiffness properties that connects two subsystems A and B. The residual subsystem R becomes:

$$\mathbf{Y}^{\mathrm{R}} = \begin{bmatrix} \mathbf{Y}^{\mathrm{A}} & \\ & \mathbf{Y}^{\mathrm{B}} \end{bmatrix} \tag{8}$$

The dynamic behavior of the joint J can be obtained by removing the dynamics of substructures A and B from the dynamic behavior of the assembled structure AJB as shown in Figure 1. It can be noted that the

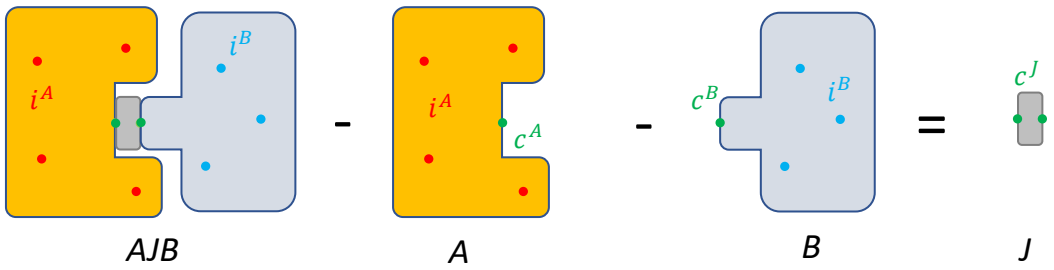

Figure 1: Joint identification through direct decoupling. The unknown subsystem J has only coupling DoFs c.

unknown subsystem J is defined only on the set of coupling DoFs c. When these coupling DoFs are not accessible for measurements in the whole system AJB, expansion techniques allow to obtain the corresponding FRFs from information contained in the internal DoFs of the system AJB.

2.2 System Equivalent Model Mixing

The SEMM is a technique developed in the frequency based substructuring frame to expand the information measured at some DoFs m of a component, on some DoFs only present in its numerical model. At the end, the considered component is described by a hybrid model in which the FRFs of inaccessible DoFs are available.

The different models involved in the expansion process are described below:

- *parent model* $\mathbf{Y}^{\mathrm{par}}$: the numerical model of the component defined on the global set of DoFs g;

- *overlay model* $\mathbf{Y}^{\text{ov}}$: the experimental model of the component obtained by measuring and exciting on the measurement DoFs m

$$\mathbf{Y}^{\text{ov}} = \mathbf{Y}^{\text{ov}}_{\text{mm}} \tag{9}$$

- *removed model* $\mathbf{Y}^{\text{rem}}$: a numerical condensed form of the parent model. In the so called "Extended SEMM" [6], the removed model is defined on the global set of DoFs g and coincides with the parent model:

$$\mathbf{Y}^{\text{rem}} = \mathbf{Y}^{\text{rem}}_{\text{gg}} \tag{10}$$

- *hybrid model* $\overline{\mathbf{Y}}^{\text{hyb}}$: the resulting model. This is defined on the same DoFs of the parent model. For the Extended SEMM equation, specified for the global set of DoFs g, it is [7]:

$$\overline{\mathbf{Y}}^{\text{hyb}} = \mathbf{Y}^{\text{par}}_{\text{gg}} - \mathbf{Y}^{\text{par}}_{\text{gg}}(\mathbf{Y}^{\text{par}}_{\text{mg}})^{+}\mathbf{Y}^{\text{par}}_{\text{mm}}(\mathbf{Y}^{\text{par}}_{\text{gm}})^{+}\mathbf{Y}^{\text{par}}_{\text{gg}} + \mathbf{Y}^{\text{par}}_{\text{gg}}(\mathbf{Y}^{\text{par}}_{\text{mg}})^{+}\mathbf{Y}_{\text{ov}}(\mathbf{Y}^{\text{par}}_{\text{gm}})^{+}\mathbf{Y}^{\text{par}}_{\text{gg}} \tag{11}$$

The expansion technique is schematically depicted in Figure 2.

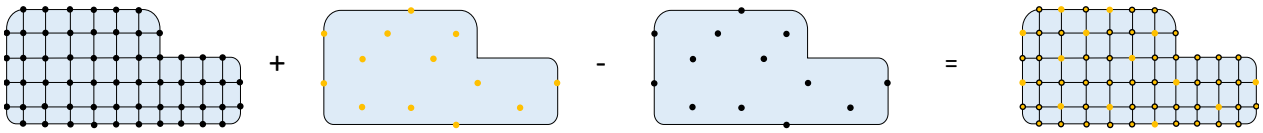

parent model overlay model removed model hybrid model

Figure 2: SEMM expansion technique. In the numerical parent model, that provides the global set of DoFs of the component, the dynamics measured on the DoFs of the experimental overlay model are overlapped. The dynamics of the numerical model are then subtracted by decoupling the removed model.

Note that in Eq. (11) the matrix product $(\mathbf{Y}_{\text{gm}})^{+}\mathbf{Y}_{\text{gg}}$ condenses the dynamics of the global set of DoFs g to the set of DoFs m. In particular, the FRFs $\mathbf{Y}_{\text{gm}}$ relates the response $\mathbf{u}_{\text{g}}$ at the global set of DoFs g of the parent model, to a set of forces $\mathbf{g}_{\text{m}}$ applied to the set of DoFs m:

$$\mathbf{g}_{\text{m}} = (\mathbf{Y}_{\text{gm}})^{+}\mathbf{u}_{\text{g}} \tag{12}$$

The matrix product $\mathbf{Y}_{\text{gg}}(\mathbf{Y}_{\text{mg}})^{+}$ expands the dynamics of the set of DoFs m to the global set of DoFs g. In particular, the FRF $\mathbf{Y}_{\text{mg}}$ relates the response $\mathbf{u}_{\text{m}}$ at the set of DoFs m, with the forces $\tilde{\mathbf{g}}_{\text{g}}$ at the global set of DoFs g:

$$\tilde{\mathbf{g}}_{\text{g}} = (\mathbf{Y}_{\text{mg}})^{+}\mathbf{u}_{\text{m}} \tag{13}$$

The two matrix products applied to the FRF $\mathbf{Y}^{\text{par}}_{\text{mm}}$ of parent model at the DoFs m gives the removed model, while when they are applied to the overlay model $\mathbf{Y}_{\text{ov}}$, add the measured dynamics to the parent model.

2.3 Joint identification procedure

The joint identification procedure is developed considering that the coupling DoFs are not accessible for measurements. To perform decoupling, FRFs of the assembled system AJB at the coupling DoFs c are necessary, thus SEMM expansion technique can be used. In this way, the dynamic behavior of the joint J is identified using the hybrid model of the whole system AJB containing the coupling DoFs c and the hybrid models of subsystems A and B in the decoupling procedure. However, to obtain the hybrid model of the whole system AJB, a parent model is needed. This can be obtained by coupling the hybrid models of the subsystems A and B with an initial guess model of the joint J. Since the real model of the joint J is unknown, the procedure is iterative. The coupling procedure is performed similarly to the decoupling one

described in Section 2.1, by setting in Eq. (7):

$$\mathbf{Y}_{\mathrm{i+1}} = \begin{bmatrix} \mathbf{Y}^{\mathrm{A,hyb}} & & \\ & \mathbf{Y}^{\mathrm{J}}_{\mathrm{i}} & \\ & & \mathbf{Y}^{\mathrm{B,hyb}} \end{bmatrix} \tag{14}$$

in which $\mathbf{Y}^{\mathrm{J}}_{\mathrm{i}}$ is the joint FRF at iteration i. Note that in coupling procedure, compatibility and equilibrium in Eq. (3) and (4), must be satisfied at all the coupling DoFs. Moreover, at the first iteration, a guess model $\mathbf{Y}^{\mathrm{J}}_{0}$ of the joint must be provided. By performing a SEMM expansion on the parent model $\mathbf{Y}^{\mathrm{AJB,par}}_{\mathrm{i+1}}$, using the experimental overlay model $\mathbf{Y}^{\mathrm{AJB,ov}}$, the hybrid model $\mathbf{Y}^{\mathrm{AJB,hyb}}_{\mathrm{i+1}}$ is obtained. At this point, the decoupling can be performed in order to find a model for the joint $\mathbf{Y}^{\mathrm{J}}_{\mathrm{i+1}}$. This model is used in (14) at the following iterative step, in order to reach convergence. The iterative algorithm stops when the following convergence criterion is satisfied:

$$\frac{\left|(\mathbf{Y}^{\mathrm{AJB,par}}_{\mathrm{mm}})_{\mathrm{i+1}} - \mathbf{Y}^{\mathrm{AJB,ov}}\right|_2}{\left|\mathbf{Y}^{\mathrm{AJB,ov}}\right|_2} < \varepsilon \tag{15}$$

i.e., when the parent model at iteration i+1 and the overlay model are very close on the set of measurement DoFs m. By looking at Eq. (11), this means that the SEMM expansion cannot further update the parent model. The FRF matrix of the identified joint $\mathbf{Y}^{\mathrm{J}}$ shows the dynamic behavior of the joint and in particular its natural frequencies. Also, by inverting this matrix, it is possible to obtain the corresponding dynamic stiffness matrix $\mathbf{Z}^{\mathrm{J}}$ useful to identify the physical properties of the joint.

In [7], to reach convergence in a less number of iterations, it is proposed to use a weighted pseudo-inverse of the matrices $\mathbf{Y}^{\mathrm{AJB,par}}_{\mathrm{mg}}$ and $\mathbf{Y}^{\mathrm{AJB,par}}_{\mathrm{gm}}$ in Eq. (11), assigning to the coupling DoF c a much higher weight than the other DoFs. A weighting matrix $\mathbf{W}$, to assign a different weight w_{m}, w_{v} and w_{c} to the different sets of DoFs, can be defined as follows:

$$\mathbf{W} = \begin{bmatrix} \mathbf{w}_{\mathrm{m}} & & \\ & \mathbf{w}_{\mathrm{v}} & \\ & & \mathbf{w}_{\mathrm{c}} \end{bmatrix} = \begin{bmatrix} w_{\mathrm{m}}\mathbf{I}_{\mathrm{mm}} & & \\ & w_{\mathrm{v}}\mathbf{I}_{\mathrm{vv}} & \\ & & w_{\mathrm{c}}\mathbf{I}_{\mathrm{cc}} \end{bmatrix} \tag{16}$$

and the two pseudo-inverses $(\mathbf{Y}^{\mathrm{par}}_{\mathrm{mg}})^{+}$ and $(\mathbf{Y}^{\mathrm{par}}_{\mathrm{gm}})^{+}$ are computed as:

$$(\mathbf{Y}_{\mathrm{mg}})^{+} = \mathbf{W}\mathbf{Y}^{H}_{\mathrm{mg}}(\mathbf{Y}_{\mathrm{mg}}\mathbf{W}\mathbf{Y}^{H}_{\mathrm{mg}})^{-1} \tag{17}$$

$$(\mathbf{Y}_{\mathrm{gm}})^{+} = (\mathbf{Y}^{H}_{\mathrm{gm}}\mathbf{W}\mathbf{Y}_{\mathrm{gm}})^{-1}\mathbf{Y}^{H}_{\mathrm{gm}}\mathbf{W} \tag{18}$$

where the superscripts ^{AJB} and ^{par} are omitted for clarity.

3 Improving of the conditioning of the identification procedure

The presented joint identification procedure needs matrix inversion in the SEMM expansion and in the decoupling process at each iteration. If the matrices to be inverted are ill-conditioned, the error in the data can be amplified in the solution. In order to improve the solution, it is necessary to recognize the possible sources of ill-conditioning and find some strategies to limit the error propagation in the final solution.

3.1 Role of the decoupling interface on the accuracy of the solution

A source of ill-conditioning is hidden in the decoupling step, in particular in Eq. (7) where the IFM has to be inverted. If this matrix is ill-conditioned, the identified FRFs of the unknown subsystem, here the joint J, can present a lot of spurious peaks. The conditioning of the IFM matrix depends on the chosen interface, i.e. on the DoFs where the compatibility and equilibrium are imposed [5]. In general, using the standard interface, in which only the coupling DoFs c are considered, the solution shows spurious peaks. To avoid

this issue, an extended interface is usually adopted, in which both coupling DoFs c and internal DoFs m are used. In the present problem, this type of interface shows some drawbacks. In fact, the coupling DoFs c on which compatibility is imposed, are not directly measured. The hybrid models at these DoFs are a result of an expansion procedure, so they can be affected by expansion error. Consequently, this error can propagate in the decoupling procedure if the IFM is ill-conditioned. To reduce the error in the IFM, a possible choice is to avoid the use of the coupling DoFs in the decoupling interface, i.e. to adopt a pseudo-interface. In this case, compatibility and equilibrium conditions are only imposed on the measured DoFs m.

3.2 Role of SEMM on the accuracy of the solution

Another source of ill-conditioning in the procedure can be found in the SEMM expansion performed on the assembled system AJB. In Eq. (11), two non-square matrices $\mathbf{Y}_{\text{mg}}^{\text{AJB,par}}$ and $\mathbf{Y}_{\text{gm}}^{\text{AJB,par}}$ are inverted. In principle, these sub-matrices $\mathbf{Y}_{\text{mg}}^{\text{AJB,par}}$ and $\mathbf{Y}_{\text{gm}}^{\text{AJB,par}}$ are derived from a numerical model and are not affected by errors. Instead, in the present iterative procedure, the parent model is generated by coupling the hybrid models of the subsystems A and B and the joint model identified at the previous iteration. The hybrid models of the subsystems A and B are affected by measurement noise and expansion error, while the identified joint model can be affected by the ill-conditioning of the IFM as discussed in Section 3.1. For this reason, particular care must be taken when computing the pseudo-inverse of the two matrices $\mathbf{Y}_{\text{mg}}^{\text{AJB,par}}$ and $\mathbf{Y}_{\text{gm}}^{\text{AJB,par}}$. When weights are used in the SEMM procedure as suggested in [7], the conditioning of these matrices may get worse. In fact, if the weight assigned to a particular set of DoFs is much higher than the weigth assigned to the other set, the matrix $\mathbf{W}$ and consequently the matrices $\mathbf{Y}_{\text{mg}}^{\text{AJB,par}}$ and $\mathbf{Y}_{\text{gm}}^{\text{AJB,par}}$ are ill-conditioned.

A physical meaning of the weights is given in the following, for the two pseudo inverses. The weighted pseudo-inverse defined in (18) can be rewritten as:

$$(\mathbf{Y}_{\text{gm}})^{+} = \boldsymbol{\Delta}_{\text{gm}}^{-1}\mathbf{Y}_{\text{gm}}^{H}\mathbf{W} = \begin{bmatrix} w_{\text{m}}\boldsymbol{\Delta}_{\text{gm}}^{-1}\mathbf{Y}_{\text{mm}}^{H} & w_{\text{v}}\boldsymbol{\Delta}_{\text{gm}}^{-1}\mathbf{Y}_{\text{vm}}^{H} & w_{\text{c}}\boldsymbol{\Delta}_{\text{gm}}^{-1}\mathbf{Y}_{\text{cm}}^{H} \end{bmatrix} \tag{19}$$

where

$$\boldsymbol{\Delta}_{\text{gm}} = \mathbf{Y}_{\text{gm}}^{H}\mathbf{W}\mathbf{Y}_{\text{gm}} = w_{\text{m}}\mathbf{Y}_{\text{mm}}^{H}\mathbf{Y}_{\text{mm}} + w_{\text{v}}\mathbf{Y}_{\text{vm}}^{H}\mathbf{Y}_{\text{vm}} + w_{\text{c}}\mathbf{Y}_{\text{cm}}^{H}\mathbf{Y}_{\text{cm}} \tag{20}$$

Consequently, the forces $\mathbf{g}_{\text{m}}$ in Eq. (12) are determined as:

$$\mathbf{g}_{\text{m}} = w_{\text{m}}\boldsymbol{\Delta}_{\text{gm}}^{-1}\mathbf{Y}_{\text{mm}}^{H}\mathbf{u}_{\text{m}} + w_{\text{v}}\boldsymbol{\Delta}_{\text{gm}}^{-1}\mathbf{Y}_{\text{vm}}^{H}\mathbf{u}_{\text{v}} + w_{\text{c}}\boldsymbol{\Delta}_{\text{gm}}^{-1}\mathbf{Y}_{\text{cm}}^{H}\mathbf{u}_{\text{c}} \tag{21}$$

where it can be seen that, when the weight assigned to the coupling DoFs c is much higher than the weigth assigned to the other DoFs, the forces $\mathbf{g}_{\text{m}}$ are mainly determined by the response at the coupling DoFs c of the parent model.

The weighted pseudo-inverse defined in (17) can be rewritten as:

$$(\mathbf{Y}_{\text{mg}})^{+} = \mathbf{W}\mathbf{Y}_{\text{mg}}^{H}\boldsymbol{\Delta}_{\text{mg}}^{-1} = \begin{bmatrix} w_{\text{m}}\mathbf{Y}_{\text{mm}}^{H}\boldsymbol{\Delta}_{\text{mg}}^{-1} \\ w_{\text{v}}\mathbf{Y}_{\text{mv}}^{H}\boldsymbol{\Delta}_{\text{mg}}^{-1} \\ w_{\text{c}}\mathbf{Y}_{\text{mc}}^{H}\boldsymbol{\Delta}_{\text{mg}}^{-1} \end{bmatrix} \tag{22}$$

where

$$\boldsymbol{\Delta}_{\text{mg}} = w_{\text{m}}\mathbf{Y}_{\text{mm}}\mathbf{Y}_{\text{mm}}^{H} + w_{\text{v}}\mathbf{Y}_{\text{mv}}\mathbf{Y}_{\text{mv}}^{H} + w_{\text{c}}\mathbf{Y}_{\text{mc}}\mathbf{Y}_{\text{mc}}^{H} \tag{23}$$

Consequently, the forces $\tilde{\mathbf{g}}_{\text{g}}$ defined in Eq. (13) are determined as:

$$\tilde{\mathbf{g}}_{\text{g}} = \begin{bmatrix} \tilde{\mathbf{g}}_{\text{m}} \\ \tilde{\mathbf{g}}_{\text{v}} \\ \tilde{\mathbf{g}}_{\text{c}} \end{bmatrix} = \begin{bmatrix} w_{\text{m}}\mathbf{Y}_{\text{mm}}^{H}\boldsymbol{\Delta}_{\text{mg}}^{-1}\mathbf{u}_{\text{m}} \\ w_{\text{v}}\mathbf{Y}_{\text{mv}}^{H}\boldsymbol{\Delta}_{\text{mg}}^{-1}\mathbf{u}_{\text{m}} \\ w_{\text{c}}\mathbf{Y}_{\text{mc}}^{H}\boldsymbol{\Delta}_{\text{mg}}^{-1}\mathbf{u}_{\text{m}} \end{bmatrix} \tag{24}$$

where it can be seen that, when the weight assigned to the coupling DoFs c is much higher than the weigth assigned to the other DoFs, the responses $\mathbf{u}_{\text{m}}$ mainly determine the forces $\tilde{\mathbf{g}}_{\text{c}}$ at the coupling DoFs c. The overall effect is that the expansion is focused on the set of DoFs c.

3.3 Consistent use of TSVD in decoupling and SEMM procedures

The effect of the weights on the conditioning of the matrices $\mathbf{Y}_{\text{mg}}^{\text{AJB,par}}$ and $\mathbf{Y}_{\text{gm}}^{\text{AJB,par}}$ can be seen by looking at the distribution of their normalized singular values σ_i/σ_1 versus frequency. When a much higher weight is assigned to the coupling DoFs c, a clear jump in the normalized singular value trend at each frequency can be observed. This jump occurs after the first N_c singular values, where N_c is the number of coupling DoFs c. The weights used in SEMM have also effects on the conditioning of the Interface Flexibility Matrix in the decoupling procedure. Using an extended interface, a clear jump in the distribution of the normalized singular values σ_i/σ_1 of the IFM is observed. In particular, a number N_m of singular values (being N_m the number of measurement DoFs m) are dominant, while the remaining N_c are nearly zero. It can be noted that the jump in the distribution of the normalized singular values of the IFM depends on the value of the weight introduced in the SEMM procedure. The IFM is strongly ill-conditioned and the identified FRFs of the joint J present a lot of spurious peaks. To improve the solution, the TSVD can be used to truncate the smallest N_c singular values in the inversion of the IFM. Note that this seems to be equivalent of using a pseudo-interface in the decoupling process without applying any weight in the SEMM expansion and without truncating the singular values of the IFM.

A different strategy can be adopted by using the TSVD also in the matrices $\mathbf{Y}_{\text{mg}}^{\text{AJB,par}}$ and $\mathbf{Y}_{\text{gm}}^{\text{AJB,par}}$ in the SEMM procedure. In [10], the use of TSVD to improve the hybrid model of a component is suggested but the number of singular values to be truncated is chosen in a heuristic way. Here, a clear indication about the number of singular values to be truncated in the inversion of matrices $\mathbf{Y}_{\text{mg}}^{\text{AJB,par}}$ and $\mathbf{Y}_{\text{gm}}^{\text{AJB,par}}$ is given by analyzing the distribution of their normalized singular values σ_i/σ_1 versus frequency. The number of singular values to be retained is equal to the number of weighted coupling DoFs N_c. Note that, when some singular values are truncated, a discrepancy between the overlay model and the SEMM hybrid model at the DoFs m occurs. Moreover, by looking at the distribution of normalized singular values of the IFM, when weights and TSVD are used in the SEMM procedure, it can be seen that now only N_c singular values are dominant, while the other N_m are nearly zero. Again, the IFM is strongly ill-conditioned but it is possible to improve the identified FRFs of the joint model J by truncating the smallest N_m singular values.

3.4 Estimation of the mass, damping and stiffness matrices of the identified joint

The proposed strategies aim to improve the identification of the joint FRFs by reducing ill-conditioning. However, spurious peaks can still be present that make difficult the estimation of joint properties. The dynamic stiffness matrix $\mathbf{Z}^{\text{J}}$ of the identified joint, obtained through the inversion of the FRF matrix $\mathbf{Y}^{\text{J}}$ is also affected by error but it mantains important physical information. Therefore, it can be convenient to fit each single term $\mathbf{Z}_{hk}^{J}$ of the identified dynamic stiffness matrix with three parameters m_{hk}^{J}, c_{hk}^{J} and k_{hk}^{J} that represents, respectively, the mass, damping and stiffness coefficients associated to the pair of DoFs h and k. The estimated matrices of mass $\mathbf{M}_{est}^{J}$, damping $\mathbf{C}_{est}^{J}$ and stiffness $\mathbf{K}_{est}^{J}$ can be used to express the dynamic stiffness matrix $\mathbf{Z}_{est}^{J}$ and through its inversion, the FRF matrix $\mathbf{Y}_{est}^{J}$ of the joint model:

$$\mathbf{Z}_{est}^{J} = -\omega^2\mathbf{M}_{est}^{J} + j\omega\mathbf{C}_{est}^{J} + \mathbf{K}_{est}^{J} \tag{25}$$

$$\mathbf{Y}_{est}^{J} = -\omega^2(\mathbf{Z}_{est}^{J})^{-1} \tag{26}$$

The FRF matrix in Eq. (26) represents a filtered solution for the joint model and can be used to predict the dynamic behavior of the assembled system $\mathbf{Y}_{est}^{AJB}$. In this way, it is possible to obtain a better estimation of both the FRFs and the physical properties of the joint.

4 Laboratory testbed

The assembled system, shown in Fig. 3(a), is composed by two steel beams A and B connected through an elastic joint J (see Fig. 3(b)). The whole system is suspended to soft springs to simulate free-free conditions. This elastic joint is designed to allow the possibility of assembling and disassemblig the system. The joint

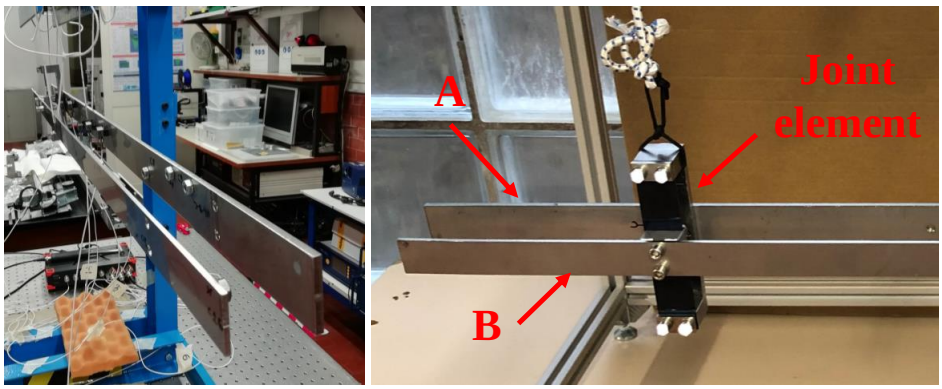

(a) Assembled system (b) Joint element

Figure 3: Experimental setup

itself can be considered as a subsystem whose dynamic behavior can be experimentally determined. The beams have length of 1 m and cross-section of 40 mm $\times$ 5 mm and 30 mm $\times$ 3 mm respectively. The joint element is connected to the beams at a distance of 0.2 m from one of their ends.

To perform the identification procedure, it is necessary to evaluate the hybrid models of the whole system AJB and of the two beams A and B. For this purpose, their parent and overlay models and a model of the joint J has to be defined. The parent models of the two beams are obtained starting from FE models using solid elements. The contact surface between each beam and the joint is modeled through remote points in order to retain the local flexible behavior. The Mode Superposition Method is used to compute the numerical FRFs. The overlay models are experimentally determined on a set of 9 measurement DoFs m for each beam. Two additional measurement DoFs are considered as validation DoFs v. The FRFs of the assembled system and of the two single beams are determined up to 200 Hz by using an impulse excitation and measuring the accelerations at each considered DoF. Measurements are performed only in the z-direction normal to the contact surface between the beams and the joint.

The choice of the joint model is crucial. It must be able to reproduce the dynamic behavior of the real joint, using only meaningful DoFs. Moreover, it is convenient to limit the number of coupling DoFs c because the decoupling process requires that the number of coupling DoFs c has to be equal or less to the number of measured DoFs m. The joint model is defined at the two remote points where it is connected to the beams and each remote point has three DoFs, the translation in z-direction and the rotations θ_x and θ_y around the x and y axis respectively. The total number of coupling DoFs N_c is 6. The elastic joint is measured in z-direction at the connecting points with the two beams to obtain experimental FRFs that can be compared to the estimated ones after the identification process.

5 Results

In this Section, the results of the joint identification procedure performed on the testbed are discussed.

As first, some considerations are made regarding the identification process when neither weights on coupling DoFs c, nor TSVD in SEMM and decoupling procedures are used. In this case it can be seen that, in the decoupling procedure, the conditioning of the IFM depends on the selected interface type. The distribution of the normalized singular values σ_i/σ_1 of the IFM at the first iteration are reported for some frequencies in Fig. 4. In Fig. 4(a), an extended interface with the 6 coupling DoFs c and 18 measured DoFs m is considered, while in Fig. 4(b), a pseudo-interface with only 18 measured DoFs m is considered. It is clear that the conditioning of the IFM using extended-interface is worse than using pseudo-interface. In the first case, the trend of the normalized singular values shows a clear change in slope at the 18th singular value: the last 6 normalized singular values are very small thus providing a solution (not shown in the paper) where input error is largely amplified.

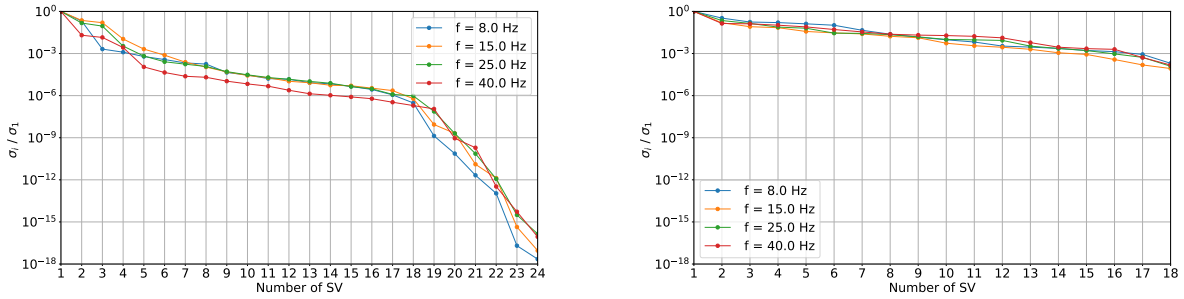

(a) Extended-interface (b) Pseudo-interface

Figure 4: Distribution of σ_i/σ_1 of IFM at some frequencies for the first iteration.

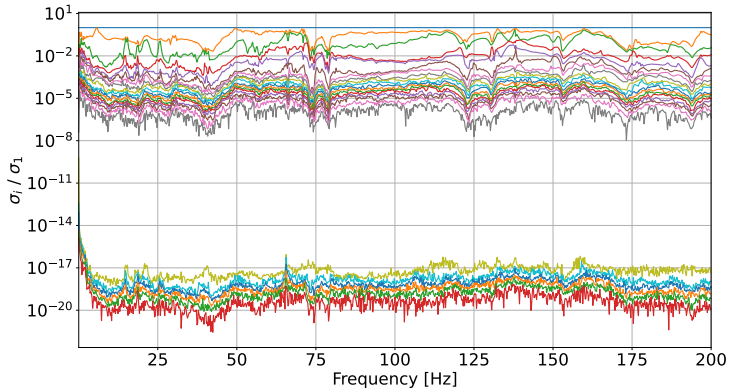

Figure 5: Frequency distribution of σ_i/σ_1 of the IFM at the first iteration. Each curve corresponds to a singular value. Weights $w_\mathrm{m} = w_\mathrm{v} =$ 1e-8 and $w_\mathrm{c} = 1$ are used in the SEMM process.

When using an extended interface for the decoupling, it is possible to obtain a more meaningful solution by assigning a much higher weight to the coupling DoFs c of the assembled structure when performing the SEMM expansion. The use of weights changes the frequency distribution of the normalized singular values of the IFM, as shown in Fig. 5, where the weights used are $w_\mathrm{m} = w_\mathrm{v} =$ 1e-8 and $w_\mathrm{c} = 1$. It can be noted that a clear jump in the distribution of the singular values arises at all frequencies. In particular, the last 6 singular values are nearly zero. These singular values make the IFM strongly ill-conditioned. The

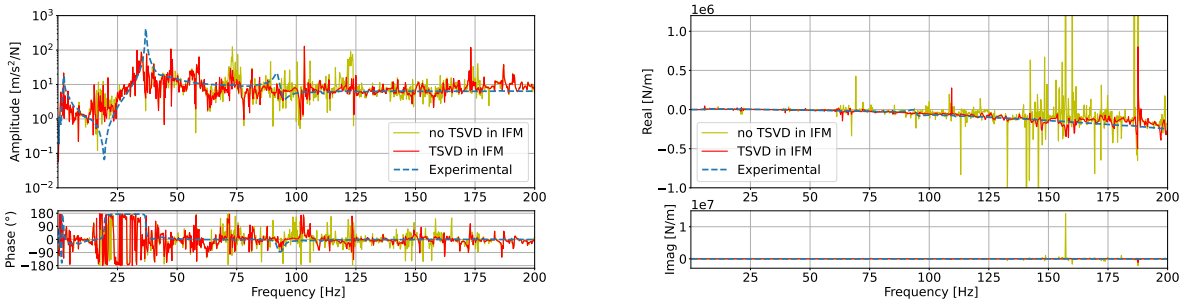

(a) Accelerance FRF (b) Dynamic Stiffness

Figure 6: Results of the joint identification: (a) drive point FRF $\mathbf{Y}^\mathrm{J}$ at DoF q_{2z}; (b) dynamic stiffness $\mathbf{Z}^\mathrm{J}$ at DoF q_{2z}. Weights $w_m = w_v =$ 1e-8 and $w_c = 1$ are used in SEMM expansion.

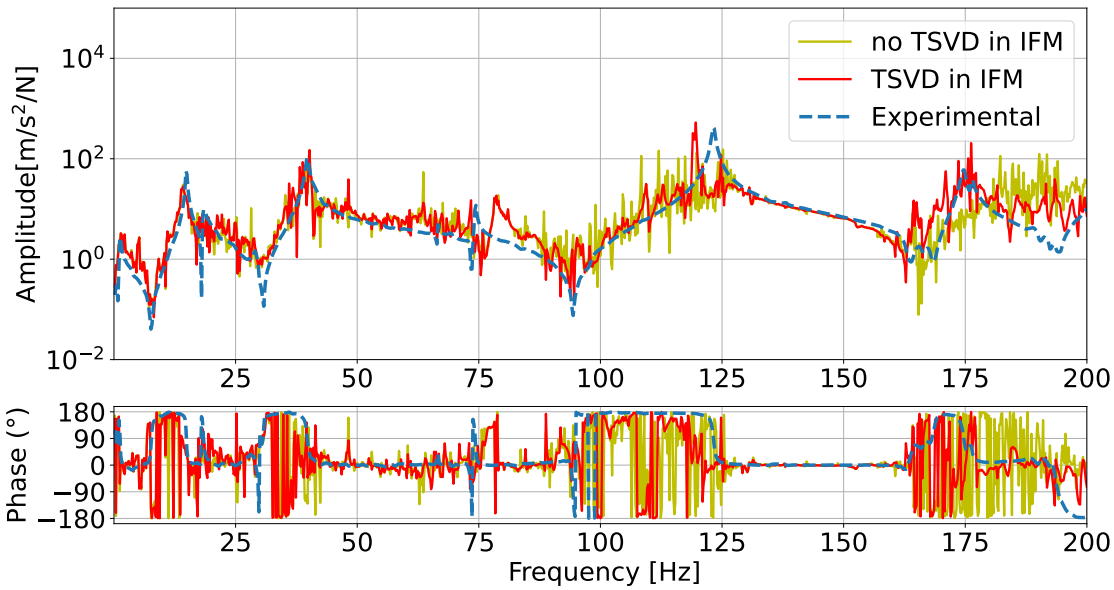

Figure 7: Drive point FRF of assembled system at the DoF v_{1z} on beam B reconstructed with the identified joint. Weights $w_{\mathrm{m}} = w_{\mathrm{v}} =$ 1e-8 and $w_{\mathrm{c}} = 1$ are used in SEMM expansion.

TSVD can be used in decoupling to eliminate the last 6 singular values of the IFM. In Fig. 6(a), the drive point FRF of the joint at the connection DoF q_{2z} is shown: the identified FRF without using TSVD and the identified FRF using TSVD are compared with the experimental one. In Fig. 6(b), the dynamic stiffness of the joint at the connection DoF q_{2z} is shown: the identified impedance without using TSVD and the identified impedance using TSVD are compared with the one derived from experimental measurements. In both figures, the results using TSVD are less prone to error amplification, but anyway the identification is not satisfactory. The two identified FRF matrices of the joint can be used to reconstruct the drive point FRF of the validation DoFs v_{1z}. In Fig. 7, the drive point FRF of the assembled system at the validation DoF v_{1z} of beam B is shown: the reconstructed FRF using joint identified without using TSVD and the reconstructed FRF using joint identified using TSVD are compared with the experimental one. Both the solutions show a lot of spurious peaks and it is difficult to distinguish the relevant dynamics of the assembled system.

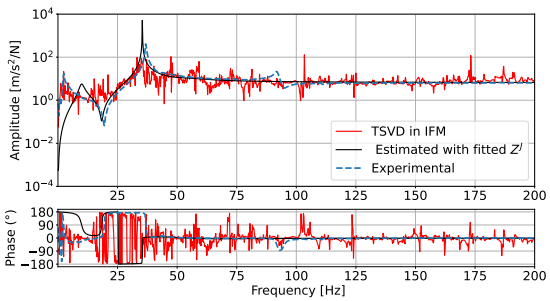

(a) Accelerance FRF

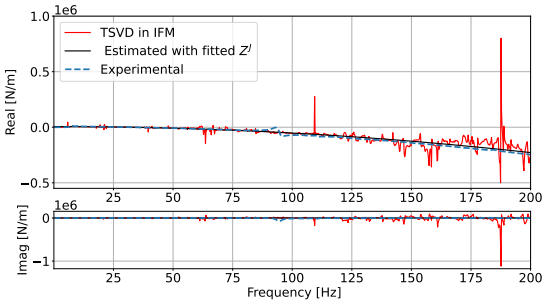

(b) Dynamic Stiffness

Figure 8: Results of the joint identification: (a) drive point FRF $\mathbf{Y}^{\mathrm{J}}$ at DoF q_{2z}; (b) dynamic stiffness $\mathbf{Z}^{\mathrm{J}}$ at DoF q_{2z}. Weights $w_{\mathrm{m}} = w_{\mathrm{v}} =$ 1e-8 and $w_{\mathrm{c}} = 1$ are used in SEMM expansion.

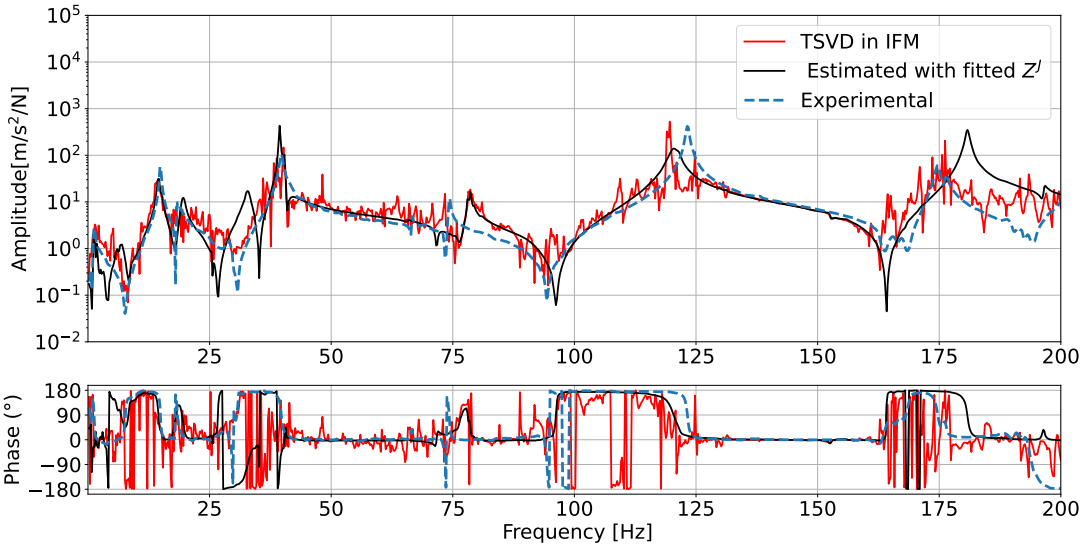

Figure 9: Drive point FRF of assembled system at the DoF v_{1z} on beam B reconstructed with the identified joint or estimated with fitted $\mathbf{Z}^{\mathrm{J}}$. Weights $w_{\mathrm{m}} = w_{\mathrm{v}} =$ 1e-8 and $w_{\mathrm{c}} = 1$ are used in SEMM expansion.

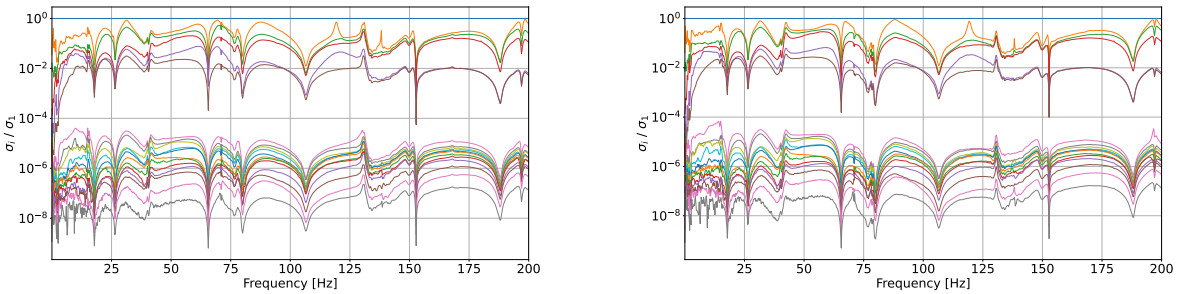

(a) $\mathbf{Y}_{\mathrm{mg}}^{\mathrm{AJB,par}}$ (b) $\mathbf{Y}_{\mathrm{gm}}^{\mathrm{AJB,par}}$

Figure 10: Frequency distribution of σ_i/σ_1 of SEMM matrices at the first iteration. Each curve corresponds to a singular value. Weights $w_{\mathrm{m}} = w_{\mathrm{v}} =$ 1e-8 and $w_{\mathrm{c}} = 1$ are used in the SEMM process.

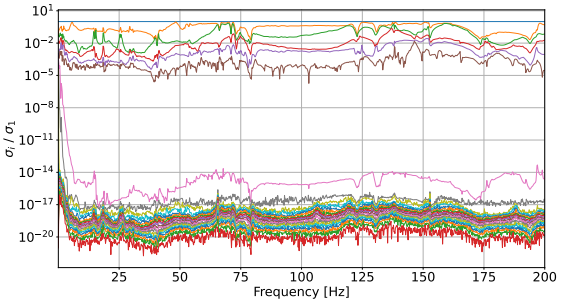

Figure 11: Frequency distribution of σ_i/σ_1 of the IFM at the first iteration. Each curve corresponds to a singular value. Weights $w_{\mathrm{m}} = w_{\mathrm{v}} =$ 1e-8 and $w_{\mathrm{c}} = 1$ and TSVD are used in the SEMM process

However, it is possible to further improve the quality of the identified FRF matrix of the joint by estimating the mass $\mathbf{M}_{est}^{J}$, damping $\mathbf{C}_{est}^{J}$ and stiffness $\mathbf{K}_{est}^{J}$ matrices of the joint from the identified dynamic stiffness

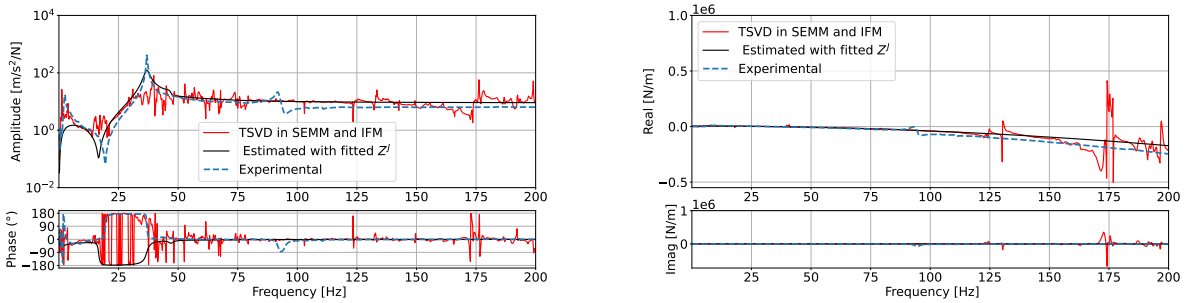

(a) Accelerance FRF

(b) Dynamic Stiffness

Figure 12: Results of the joint identification: (a) drive point FRF $\mathbf{Y}^{\mathrm{J}}$ at DoF q_{2z}; (b) dynamic stiffness $\mathbf{Z}^{\mathrm{J}}$ at DoF q_{2z}. Weights $w_{\mathrm{m}} = w_{\mathrm{v}} =$ 1e-8 and $w_{\mathrm{c}} = 1$ are used in SEMM expansion.

matrix as proposed in Section 3.4. These matrices $\mathbf{M}^J_{est}$, $\mathbf{C}^J_{est}$ and $\mathbf{K}^J_{est}$ are used to reconstruct the dynamic stiffness $\mathbf{Z}^J_{est}$ and the FRF matrix $\mathbf{Y}^J_{est}$ of the joint. In Fig. 8(a), the drive point FRF of the joint at the connection DoF q_{2z} is shown: the identified FRF using TSVD and the estimated FRF $\mathbf{Y}^J_{est}$ are compared with the experimental one. In Fig. 8(b), the dynamic stiffness of the joint at the connection DoF q_{2z} is shown: the identified impedance using TSVD and the estimated impedance $\mathbf{Z}^J_{est}$ are compared with the one derived from experimental measurements. It can be seen that the estimated dynamic stiffness $\mathbf{Z}^J_{est}$ of the joint is in good agreement with the measured data and does not present spurious peaks. The estimated FRF $\mathbf{Y}^J_{est}$ shows a clear improvement and the resonance frequency at 36 Hz is identified, while the first resonance frequency at 2.3 Hz is not correctly identified. The estimated joint FRF matrix $\mathbf{Y}^J_{est}$ can be used to reconstruct the drive point FRF of the validation DoFs v_{1z}. In Fig. 9, the drive point FRF of the assembled system at the validation DoF v_{1z} of beam B is shown: the reconstructed FRF using joint identified using TSVD and the estimated FRF are compared with the experimental one. The FRF derived from the estimated joint seems to be not affected by error propagation, but shows some discrepancies at some frequencies.

As suggested in Section 3.3, a different strategy can be adopted by using the TSVD not only in the IFM, but also in the matrices $\mathbf{Y}^{\mathrm{AJB,par}}_{\mathrm{mg}}$ and $\mathbf{Y}^{\mathrm{AJB,par}}_{\mathrm{gm}}$ of Eq. (11) in the SEMM procedure. In fact, the use of weights in the SEMM expansion does not only affect the distribution of the normalized singular values in the IFM, but also the distribution of the normalized singular values of the two matrices $\mathbf{Y}^{\mathrm{AJB,par}}_{\mathrm{mg}}$ and $\mathbf{Y}^{\mathrm{AJB,par}}_{\mathrm{gm}}$ in Eq. (11) as shown in Fig. 10 at the first iteration of the procedure. The assigned weights are always $w_{\mathrm{m}} = w_{\mathrm{v}} =$ 1e-8 and $w_{\mathrm{c}} = 1$. As expected, a clear jump in the distribution of the normalized singular values arises at all frequencies. The first N_c normalized singular values are more relevant than the other ones. This suggests to use the TSVD in these two matrices, and retain only the first 6 singular values. Consequently, in this case, a different IFM is obtained. In Fig.11 the distribution of the normalized singular values of the IFM is shown where it can be noted that now only 6 singular values are relevant. The results obtained using TSVD in the matrices $\mathbf{Y}^{\mathrm{AJB,par}}_{\mathrm{mg}}$ and $\mathbf{Y}^{\mathrm{AJB,par}}_{\mathrm{gm}}$ and in the IFM are shown in Fig. 12 and 13 where also the results obtained by fitting the dynamic stiffness matrix $\mathbf{Z}^J$ of the joint J are shown. In particular, in Fig. 12(a), the drive point FRF of the joint at the connection DoF q_{2z} is shown: the identified FRF using TSVD in both SEMM matrices and IFM and the estimated FRF $\mathbf{Y}^J_{est}$ are compared with the experimental one. In Fig. 12(b), the dynamic stiffness of the joint at the connection DoF q_{2z} is shown: the identified impedance using TSVD in both SEMM matrices and IFM and the estimated impedance $\mathbf{Z}^J_{est}$ are compared with the one derived from experimental measurements. It can be noted that in both cases, the dynamic stiffness is in good agreement with the reference experimental one. Nonetheless, the identified joint FRF using TSVD in both SEMM matrices and in IFM, is less affected by error propagation, but it is not able to show the characteristics of its dynamic behavior. Instead, in the joint FRF $\mathbf{Y}^J_{est}$ obtained fitting the identified dynamic stiffness, the resonance frequency at 36 Hz is well estimated and the resonance frequency at 2.3 Hz is better estimated than the corresponding curve in Fig. 8. The estimated joint FRF matrix can be used to reconstruct the drive point FRF of the validation DoFs v_{1z}. In Fig. 13, the drive point FRF of the assembled system at the validation DoF v_{1z} of beam B is shown: the reconstructed FRF joint identified using TSVD in both SEMM matrices

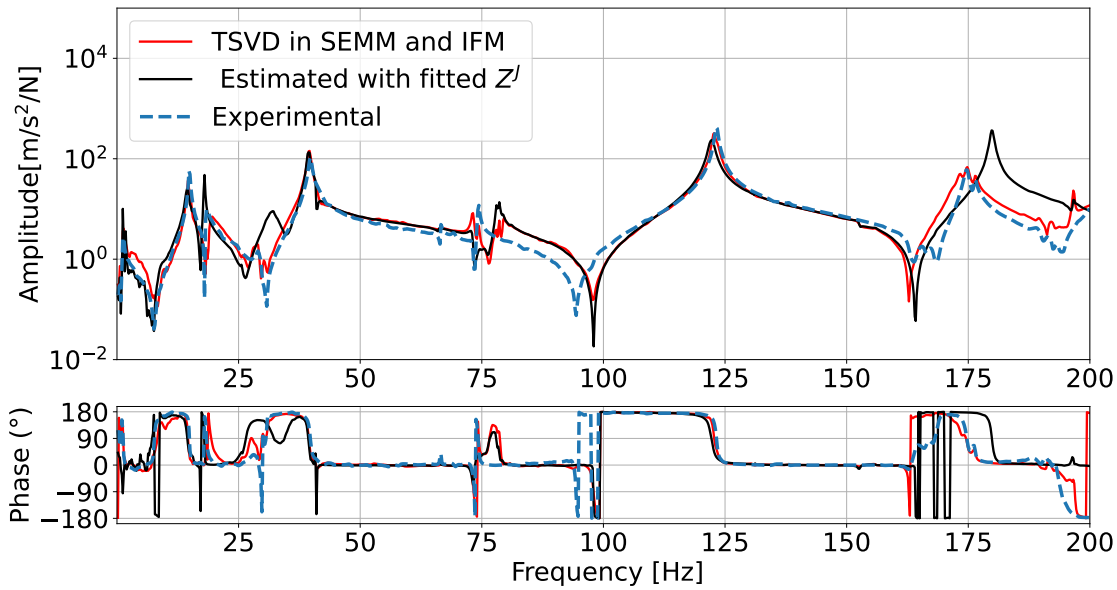

Figure 13: Drive point FRF of assembled system at the DoF v_{1z} on beam B reconstructed with the identified joint or estimated with fitted $\mathbf{Z}^{\mathrm{J}}$. Weights $w_{\mathrm{m}} = w_{\mathrm{v}} =$ 1e-8 and $w_{\mathrm{c}} = 1$ are used in SEMM expansion.

and in IFM and the estimated FRF are compared with the experimental one. It can be noted that in both cases the FRFs are in good agreement with the experimental one. These solutions seem to better predict the dynamic behavior of the assembled system with respect to the previous results.

6 Conclusions

In this work, a SEMM-based joint identification procedure is described: it provides the FRFs of the unknown joint from which the dynamic stiffness matrix can be obtained by an inversion procedure. Since results are typically affected by noise, the main sources of ill-conditioning are analyzed.

Specifically, the effect of different types of decoupling interfaces on the estimation of the joint FRFs is analyzed: it is shown that the pseudo interface can be preferred since no expansion errors are introduced in the interface flexibility matrix.

Moreover, the role of the weighted pseudo-inverse proposed in [7] on the conditioning of the procedure is investigated by analyzing the effect of the weights on the matrices to be inverted. In particular, when the weigth assigned to a particular set of DoFs is much higher than the weigth assigned to the other set, the conditioning of the matrices gets worse. This affects also the conditioning of the interface flexibility matrix in the decoupling procedure.

Therefore, some strategies to limit the error propagation in the solution are proposed. In particular, both in decoupling and SEMM procedures, it is possible to forecast that when using weigths, singular values present a clear jump. This provides an indication about the appropriate number of singular values to be retained using truncated SVD.

Finally, a fitting of the dynamic stiffness matrix of the identified joint is proposed: this allows to obtain a better estimation of both the FRFs and of the physical properties of the unknown joint.

The described procedure is implemented and the effectiveness of the proposed strategies is confirmed by results obtained on a laboratory testbed.

Acknowledgements

This research is supported by University of Rome La Sapienza and University of L'Aquila.

References

[1] M. R. W. Brake, *The Mechanics of Joined Structures*. Springer International Publishing, 2018.

[2] D. de Klerk, D. J. Rixen, and S. N. Voormeeren, "General Framework for Dynamic Substructuring: History, Review and Classification of Techniques," *AIAA Journal*, vol. 46, no. 5, pp. 1169–1181, 2008.

[3] W. D'Ambrogio and A. Fregolent, "Direct decoupling of substructures using primal and dual formulation," in *Linking Models and Experiments*, ser. Conference Proceedings of the Society for Experimental Mechanics Series, vol. 2, 2011.

[4] S. N. Voormeeren and D. J. Rixen, "A family of substructure decoupling techniques based on a dual assembly approach," *Mechanical Systems and Signal Processing*, vol. 27, pp. 379–396, 2012.

[5] W. D'Ambrogio and A. Fregolent, "The role of interface DoFs in decoupling of substructures based on the dual domain decomposition," *Mechanical Systems and Signal Processing*, vol. 24, no. 7, pp. 2035–2048, 2010.

[6] S. Klaassen, M. van der Seijs, and D. de Klerk, "System equivalent model mxing," *Mechanical Systems and Signal Processing*, vol. 105, pp. 90–112, 2018.

[7] Z. Saeed, S. W. B. Klaassen, C. M. Firrone, T. M. Berruti, and D. J. Rixen, "Experimental Joint Identification Using System Equivalent Model Mixing in a Bladed-Disk," *Journal of Vibration and Acoustics*, pp. 1–29, 2020.

[8] S. W. Klaassen and D. J. Rixen, "Using SEMM to Identify the Joint Dynamics in Multiple Degrees of Freedom Without Measuring Interfaces," in *Dynamic Substructures*, ser. Conference Proceedings of the Society for Experimental Mechanics Series, vol. 4. Springer, 2020, pp. 87–99.

[9] Z. Saeed, C. M. Firrone, and T. M. Berruti, "Joint identification through hybrid models improved by correlations," *Journal of Sound and Vibration*, vol. 494, p. 115889, mar 2021.

[10] S. W. Klaassen and D. J. Rixen, "The inclusion of a singular-value based filter in SEMM," in *Proceedings of the 38th International Modal Analysis Conference, A Conference on Structural Dynamics*, 2020.

[11] W. D'Ambrogio and A. Fregolent, "Substructure decoupling without using rotational DoFs: Fact or fiction?" *Mechanical Systems and Signal Processing*, vol. 72-73, pp. 499–512, may 2016.

[12] F. Latini, J. Brunetti, M. Kwarta, M. S. Allen, W. D'Ambrogio, and A. Fregolent, "Experimental results of nonlinear structure coupled through nonlinear connecting elements," in *Proceedings of ISMA 2020 - International Conference on Noise and Vibration Engineering and USD 2020 - International Conference on Uncertainty in Structural Dynamics*, 2020.

[13] F. Latini, J. Brunetti, W. D'Ambrogio, M. S. Allen, and A. Fregolent, "Nonlinear substructuring in the modal domain: numerical validation and experimental verification in presence of localized nonlinearities," *Nonlinear Dynamics*, vol. 104, no. 2, pp. 1043–1067, 2021.